ACS APPLIED MATERIALS & INTERFACES

Research Article

www.acsami.org

Low-Temperature, High-Performance Solution-Processed Thin-Film Transistors with Peroxo-Zirconium Oxide Dielectric

Jee Ho Park, Young Bum Yoo, Keun Ho Lee, Woo Soon Jang, Jin Young Oh, Soo Sang Chae, and Hong Koo Baik*

Department of Materials Science and Engineering, Yonsei University, 50 Yonsei-ro, Seodaemun-gu, Seoul, 120-749, Korea.

Supporting Information

ABSTRACT: We demonstrated solution-processed thin film transistors on a peroxo-zirconium oxide (ZrO_2) dielectric with a maximum temperature of 350 °C. The formation of ZrO_2 films was investigated by TG-DTA, FT-IR, and XPS analyses at various temperatures. We synthesized a zirconium oxide solution by adding hydrogen peroxide (H_2O_2). The H_2O_2 forms peroxo groups in the ZrO_2 film producing a dense-amorphous phase and a smooth surface film. Because of these characteristics, the ZrO_2 film successfully blocked leakage current even in annealing at 300 °C. Finally, to demonstrate that the ZrO_2 film is dielectric, we fabricated thin-film transistors (TFTs) with a solution-processed channel layer of indium zinc oxide (IZO) on ZrO_2 films at 350 °C. These TFTs had a mobility of 7.21 $cm^2/(V\ s)$, a threshold voltage (V_{th}) of 3.22 V, and a V_{th} shift of 1.6 V under positive gate bias stress.

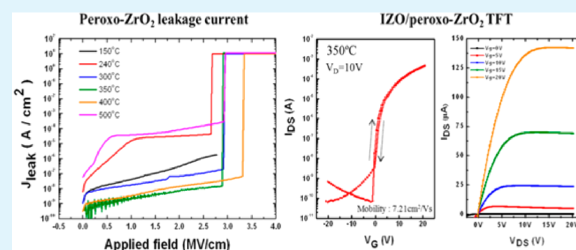

KEYWORDS: *solution process, peroxo-zirconium, thin-film transistor, hydrogen peroxide, indium zinc oxide, zirconium oxide*

1. INTRODUCTION

Recently, thin-film transistors (TFTs) made of amorphous metal oxide such as indium gallium zinc oxide (IGZO), indium zinc oxide (IZO), zinc tin oxide (ZTO), and zinc oxide (ZnO) have been extensively studied for use in active matrix liquid crystal displays (AMLCDs) and organic light-emitting diodes (OLEDs) because of their large mobility, high optical transparency, and electrical stability.[1−4] To fabricate these films at low cost using a simple method, solution processes such as inkjet printing, dip coating, and spin-coating have shown promise. However, solution-processed TFTs show reasonable electrical properties only after high-temperature annealing above 450 °C, a temperature that is incompatible with conventional TFT manufacturing processes.[5] Accordingly, a maximum annealing temperature below 350 °C has to be achieved to make use of conventional manufacturing processes for flat panel displays.[6]

To reduce the annealing temperature of solution-processed channel layers, we have introduced various methods. Most of the approaches, which include in situ hydrolysis and condensation using highly reactive metal alkoxide precursor,[1] chemical energetic combustion process through an oxidizer and fuel,[2] annealing in a high-pressure oxygen medium,[7] and zinc-hydroxo-amine complex precursors,[4] have achieved oxide TFTs with high mobility at temperature under 300 °C. However, most of these approaches have fabricated TFTs on thermally grown or vacuum-deposited SiO_2 dielectrics.

To fully integrate TFTs using a solution process, both the active layer and the dielectric layer should be formed in the same way. Several groups have reported on solution-processed dielectric layers. However, to get appropriate dielectric properties, high-temperature annealing above 500 °C is required.[8−10] Although an organic dielectric layer can form at low temperatures, most organic layers have a hydrophobic surface, which makes it difficult to coat on a layer having a, low ambient stability, and a low dielectric constant. For these reasons, the use of an organic dielectric layer for oxide TFTs has some limitations. Thus, dielectric layers should be developed and designed to operate at temperatures under 350 °C, which is the conventional flat panel display manufacturing temperature. Several groups have demonstrated oxide TFTs based on solution-processed gate dielectrics. Meyer et al. reported on a sputtered ZnO TFT with a solution-processed $Al_2PO_{5.5}$ dielectric,[11] which was successfully formed at 300 °C and had a low leakage current. However, a proper field-effect mobility of 1.5 $cm^2/(V\ s)$ could be achieved only at an annealing temperature of 600 °C. George et al. reported on solution-processed crystalline Al_2O_3 and Y_2O_3 dielectrics with crystalline ZnO TFTs with field-effect mobilies of 7 and 32 $cm^2/(V\ s)$, respectively, with annealing at 400 °C.[10] Jiang et al. described a solution-processed peroxo-HfO_2 dielectric annealed at 400 °C with a sputtered IGZO TFT and a field-effect mobility of 13.1 $cm^2/(V\ s)$.[12] Recently, Avis et al. demonstrated a ZTO TFT based on Al_2O_3 annealed at 300 °C with a field-effect mobility of 33 $cm^2/(V\ s)$.[13] However, hysteresis of ZTO TFT showed a counter clockwise behavior, indicating that the Al_2O_3 dielectric contained unknown positive or negative mobile ions. Because of this mobile ion, the capacitance of Al_2O_3 may

Received: October 29, 2012
Accepted: December 25, 2012
Published: December 25, 2012

 © 2012 American Chemical Society

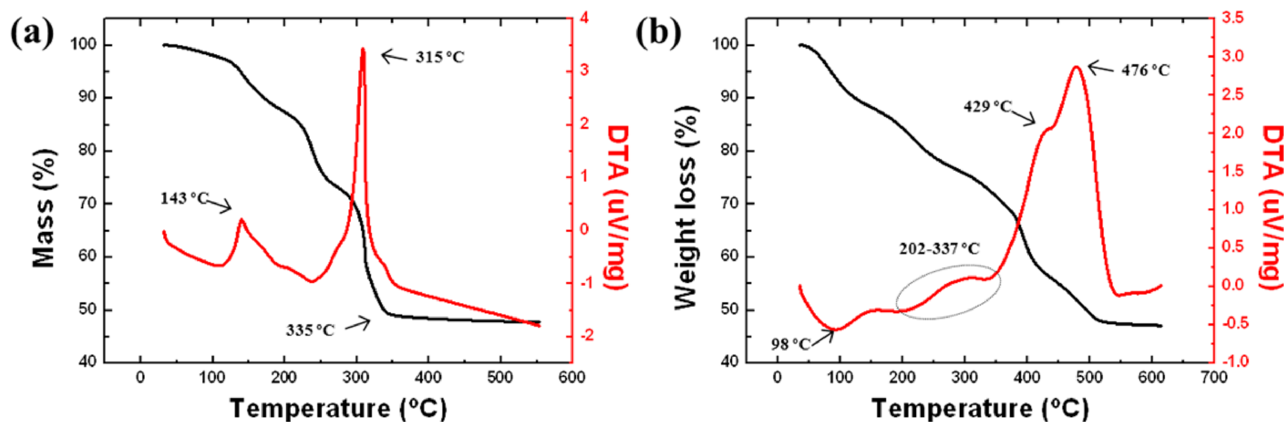

Figure 1. Thermal behavior of (a) IZO precursor dried at 130 °C and (b) ZrO_2 precursor solution at a heating rate of 10 °C/min under ambient conditions.

increase as the frequency decreases. Thus, the value for mobility in this case may be overestimated. In terms of the mobile ions in the Al_2O_3, related works have progressed. As described above, in order to fabricate a reasonable TFT with a solution-processed dielectric, heat treatment at 400 °C should be performed. Kim et al. reported on a solution-processed IZO TFT on ZrO_2 film using a high-pressure annealing method at 350 °C, and although the ZrO_2 film had low leakage current, the IZO TFT performed poorly.[14]

To overcome high-temperature annealing conditions, research on new materials is required. In this study, therefore, we proposed three strategies. First, conventional IZO films with an ethylene glycol additive for enhancing the film quality were chosen as the channel layer and metal nitrate precursor for a low decomposition temperature. Second, a zirconium dioxide (ZrO_2) dielectric layer was selected owing to its high dielectric constant (~25), wide band gap (5.1−7.8 eV), high refractive index (2.17), and transparency.[15,16] Moreover, zirconium oxychloride was adopted as a starting material because of the slow decomposition of the zirconium chloride bond. This phenomenon makes for a smooth surface. Third, hydrogen peroxide (H_2O_2) was added to the ZrO_2 solution to form peroxo-ZrO_2 films. The role of H_2O_2 was to make oxygen-rich films, allowing for greater oxidation states, and to form dense films. Using these strategies, we achieved IZO TFTs on ZrO_2 films annealed at 350 °C.

2. EXPERIMENTAL SECTION

2.1. Synthesis of IZO and ZrO_2 Solutions. For the IZO solution, 0.1 M indium nitrate hydrate [$In(NO_3)_3 \cdot xH_2O$] and 0.1 M zinc nitrate hexahydrate [$Zn(NO_3)_2 \cdot 6H_2O$] were dissolved in 2-methoxyethanol with an equivalent mole ratio of ethylene glycol. For the ZrO_2 solution, 0.2 M zirconium oxychloride ($ZrOCl_2$) was mixed with 2-methoxyethanol and then 6.67 M H_2O_2 was added. Both solutions were stirred vigorously for 12 h under ambient conditions and filtered through a 0.2 μm polytetrafluoroethylene (PTFE) syringe filter before spin coating. All of the chemical compounds were purchased from Sigma-Aldrich and used as is with no additional purification.

2.2. Metal Insulator Metal (MIM) Device Fabrication. The ZrO_2 film was deposited by spin-coating at 3000 rpm for 25 s on a heavily boron-doped silicon substrate. We adopted two steps for the annealing process: a soft bake and a hard bake. To evaporate the organic solvent, the spin-coated ZrO_2 film was soft baked at 240 °C for 5 min and then cooled to room temperature. This process was repeated 12 times. Then the film was hard baked at the intended temperature (240, 300, 350, 400, or 500 °C) for 2 h under ambient conditions. In case of the 150 °C annealed ZrO_2 film, 150 °C was chosen for both the soft and the hard bake temperature. The thicknesses for the 150, 240, 300, 350, 400, and 500 °C annealed ZrO_2 films were 368.5, 292, 223, 210, 201, and 198 nm, respectively (see Figure S1 in the Supporting Information). These film thicknesses were confirmed by spectroscopic ellipsometry (SE MG-Vis 1000, Nano View) and field-emission scanning electron microscopy (FE-SEM, JSM-7001F, JEOL) (figure S1). To characterize the ZrO_2 dielectric, we fabricated a metal insulator metal (MIM) capacitor on heavily boron-doped silicon. The capacitor was fabricated by thermally evaporating 50 nm thick circular aluminum with a shadow mask above the ZrO_2 film. The area of the circular aluminum was 0.17 mm^2.

2.3. Thin-Film Transistor Device Fabrication. We selected an inverted staggered structure for the IZO TFT on the ZrO_2 dielectric. The IZO film was produced via spin coating at 4000 rpm for 25 s on the ZrO_2 film annealed at 350 °C and subsequently annealed at 350 °C for 1 h in air. Aluminum 50 nm thick was thermally evaporated (pressure $\sim 1 \times 10^{-6}$ Torr) for a source/drain electrode with a shadow mask. The channel length and width were 150 and 1000 μm, respectively.

2.4. Film Characterization. The thermal behavior of the IZO and ZrO_2 powders, which were dried at 80 °C for 12 h, was measured by thermogravimetric differential thermal analysis (TG-DTA, Seiko Exstar 6000, Seiko) at a heating rate of 10 °C/min from room temperature to 550 °C under ambient conditions. The ZrO_2 structural information was obtained using high-resolution X-ray diffraction (HR-XRD, Ultima IV, Rigaku) with Cu Ka radiation. The film thickness and refractive index were measured by spectroscopic ellipsometry. Data were collected at incident angles of 69.8° in the range 350−850 nm. Attenuated total reflectance Fourier transform infrared spectroscopy (ATR-FT IR, Vertex 70, Bruker) was performed to investigate the chemical structure of the ZrO_2 films. The surface roughness of the ZrO_2 films was investigated by atomic force microscopy (AFM, MFP-3D-SA, Asylum Research). The chemical structure of the ZrO_2 films was measured by X-ray photoelectron spectroscopy (XPS, K-alpha, Thermo U.K.) using Al Kα radiation (1486.6 eV) and a carbon 1s peak at 284.8 eV was used as a reference for calibration.

2.5. Electrical Measurement. To investigate the electrical characterization of the ZrO_2 dielectric, the capacitance−voltage (C−V) and the leakage current density−voltage (J_{leak}−V) were measured at various annealing temperatures.

The electrical characteristics of the IZO TFT on ZrO_2 dielectric were measured in the dark at room temperature with a semiconductor parameter analyzer (Agilent E5270). The threshold voltage was determined from the saturation region by fitting a straight line to the plot of the square root of the drain current ($I_D^{1/2}$) versus the gate voltage (V_G). The saturation mobility and subthreshold slope were determined from the following equations:

$$I_D = \left(\frac{C_i W \mu_{sat}}{2L}\right)(V_G - V_{th})^2$$

dx.doi.org/10.1021/am3022625 | ACS Appl. Mater. Interfaces 2013, 5, 410−417

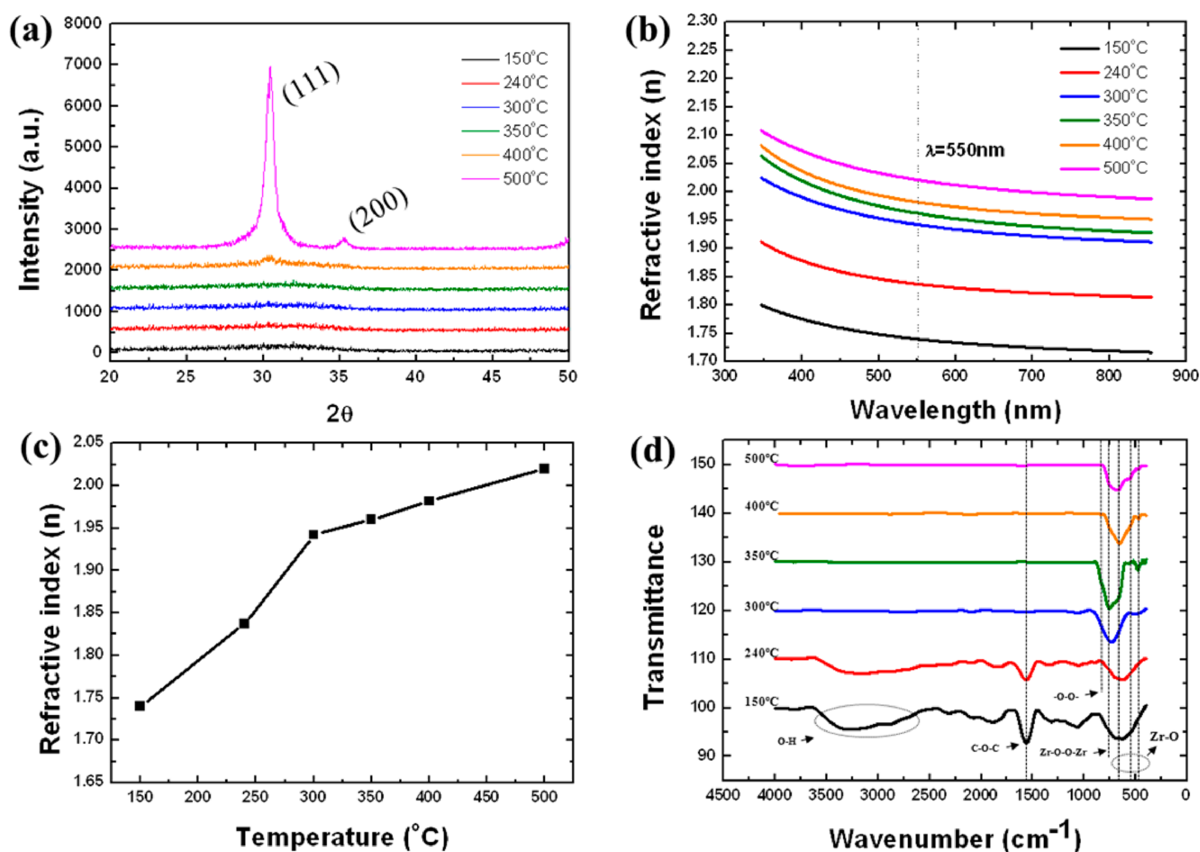

Figure 2. (a) XRD spectra, (b) refractive index, and (c) summarized refractive index values at a wavelength of 550 nm. (d) FT-IR spectroscopy of the ZrO_2 film with various annealing temperatures.

$$S = \left[\frac{d(\log_{10} I_D)}{dV_G}\right]^{-1}$$

where C_i, W, L, V_G, and V_{th} are the capacitance of the gate dielectric per unit area, the channel width, channel length, gate bias, and threshold voltage, respectively.

3. RESULTS AND DISCUSSION

To determine the heat-treatment temperature of the IZO and ZrO_2 films, thermal analysis was performed. Figure 1a shows the thermal behavior of the IZO powder. There are two exothermic peaks, one at 143 °C and the other at 315 °C, which correspond to solvent evaporation and condensation, respectively.[5] After 335 °C, significant weight loss was not observed. In order to eliminate any residual solvent, impurities, and unnecessary anion groups, we conducted thermal annealing at 350 °C for 1 h. Figure 1b shows the thermal behavior of the ZrO_2 powder. The DTA data of the ZrO_2 solution showed four peaks: a small endothermic peak at 98 °C, a broad exothermic peak from 202 to 337 °C, and large exothermic peaks at 429 and 476 °C. The small endothermic reaction at 98 °C indicates solvent evaporation and hydrolysis of the ZrO_2 solution from zirconium oxychloride to zirconium hydroxychloride. The broad exothermic peak indicates gradual densification behavior, which forms the metal oxygen metal frame, makes dense films, and decreases the impurities in the film.[5] The last two large exothermic peaks indicate the crystallization of the ZrO_2 film. Therefore, we investigated the formation of the solution-processed ZrO_2 films using various annealing temperatures and verified them with various analysis tools.

Figure 2a shows the XRD patterns of the ZrO_2 film, which was amorphous until reaching an annealing temperature of 400 °C. The 500 °C annealed ZrO_2 had a crystalline phase with (111) and (200) peaks at 30.41° and 35.25°, respectively. Conventional solution-derived ZrO_2 films crystallize at an annealing temperature of 350 °C.[18] However, the H_2O_2-added ZrO_2 film had no crystalline peak until 400 °C. In general, without H_2O_2, the metal oxide is formed from a metal hydroxide via a condensation reaction between adjoining hydroxyl groups with the removal of water. A continuous condensation reaction leads to an extended network of metal oxygen metal (M-O-M) bonds, and these M−O−M bonds in turn lead to crystalline metal oxide. In contrast, with H_2O_2, peroxo species, which are bound with metal, disturb the condensation reaction. Because there are no more sites to condense with neighboring hydroxyl groups, it is difficult to form M-O-M bonds.[17] Thus, the 400 °C annealed ZrO_2 film had an amorphous phase. The crystal size of the 500 °C annealed ZrO_2 film was calculated using the Scherrer equation to be 8.5 nm. This value is smaller than that of conventional solution-derived ZrO_2 films.[18] From this result, it is clear that hydrogen peroxide stabilizes the ZrO_2 phase until 400 °C without needing to add stabilizing dopants such as Al, Hf, and La.[19−21]

To verify the densification behavior of the ZrO_2 film, spectroscopic ellipsometry measurements were performed. The obtained refractive index (n) dispersion curves with various annealed films are shown in figure 2b. The refractive index at a wavelength of 550 nm increased from 1.74 to 2.02 as the annealing temperature increased from 150 to 500 °C. Figure 2c

dx.doi.org/10.1021/am3022625 | ACS Appl. Mater. Interfaces 2013, 5, 410−417

summarizes the refractive index values. These high refractive indices are comparable to those of vacuum-deposited films. For example, n (λ = 310 nm) = 1.82−1.92 and n (λ = 650 nm) = 2.03−2.11 have been reported for sputtered films.[15,22] The relative density can be calculated from the refractive index using the following equation[23]

$$\left(\frac{n^2 - n_2^2}{n^2 + 2n_2^2}\right)\left(\frac{n^2 + 2n_1^2}{n_1^2 - n^2}\right) = \frac{q_1}{1 - q_1}$$

$$q_1 = \frac{\rho - \rho_2}{\rho_1 - \rho_2}$$

where n, n_1, n_2, q_1, ρ, ρ_1, and ρ_2 represent the refractive index of the film, the n value of the bulk ZrO_2 (n = 2.2),[24] the number of voids in the form of air (n_2 = 1, ρ_2 = 0) or water (n_2 = 1.33, ρ_2 = 1 g/cm^3), the volume fraction of the bulk, film density, bulk ZrO_2 density (5.68 g/cm^3), and void density (air or water),[25] respectively. To determine the volume fraction, defining the exact void species in the film is necessary because the volume fraction value critically depends on n_2. We can get the n_2 value from Figure 2d. According to Figure 2d, at temperatures up to 240 °C, the annealed film contained hydroxyl groups but at temperature above 300 °C, the annealed film had no hydroxyl species in the film. The vibration peaks at around 3000−3500 cm^{-1} indicate hydroxyl species. These results mean that films below 240 °C have voids in the form of water and those above 300 °C have voids in the form of air. Considering these void types, the calculated bulk volume fractions of the 150, 240, 300, 350, 400, and 500 °C annealed films were 57.3, 67.4, 85.8, 86.8, 88.1, and 90.2%, respectively, and the relative densities were 2.68, 3.15, 4.87, 4.93, 5.00, and 5.12 g/cm^3, respectively. This result indicates that peroxo-ZrO_2 film is a dense film even at the annealing temperature of 300 °C.

To understand the chemical structure of the ZrO_2 precursor during heat treatment, FT-IR was carried out. The broad peak in the range 3000−3500 cm^{-1} indicates an O−H stretching vibration.[26] The peak at 1061 cm^{-1} was assigned as the asymmetric stretching of C−O−C in the solvent.[26] The peaks with the peroxide-zirconium complex corresponding to the O−O and Zr−O−O−Zr bonds were identified at 900 and 765 cm^{-1}, respectively.[27,28] Zr−O bonds were observed at 682, 545, and 470 cm^{-1}.[29] The 150 and 240 °C annealed films contained large amounts of solvent, peroxo-groups, and small quantities of ZrO_2. As the annealing temperature increased, the organic species in the film were eliminated and the O−H vibration of the solvent decreased. In the case of annealing temperatures above 300 °C, O−H vibration peaks were not observed and the Zr−O bond was dominant. All of the films contained peroxo species such as Zr−O−O−Zr and the 350 °C annealed film showed the largest amounts of peroxo species in the film. As the heat-treatment temperature increased, the peroxo species decreased and the Zr−O bonds increased gradually.

It is reasonable that hydrolyzed metal hydroxide converts into metal oxide at 300 °C and densification occurs continuously. Most of the solvent and unnecessary organic compounds are removed at temperatures below 240 °C and fabrication of the M−O−M frame occurs at 300 °C. This process is the same as in thermal behavior, in which gradual weight loss can be seen in the TGA results described in Figure 1b.

The chemical compositions of the ZrO_2 films were characterized by XPS and the results are shown in Figure 3.

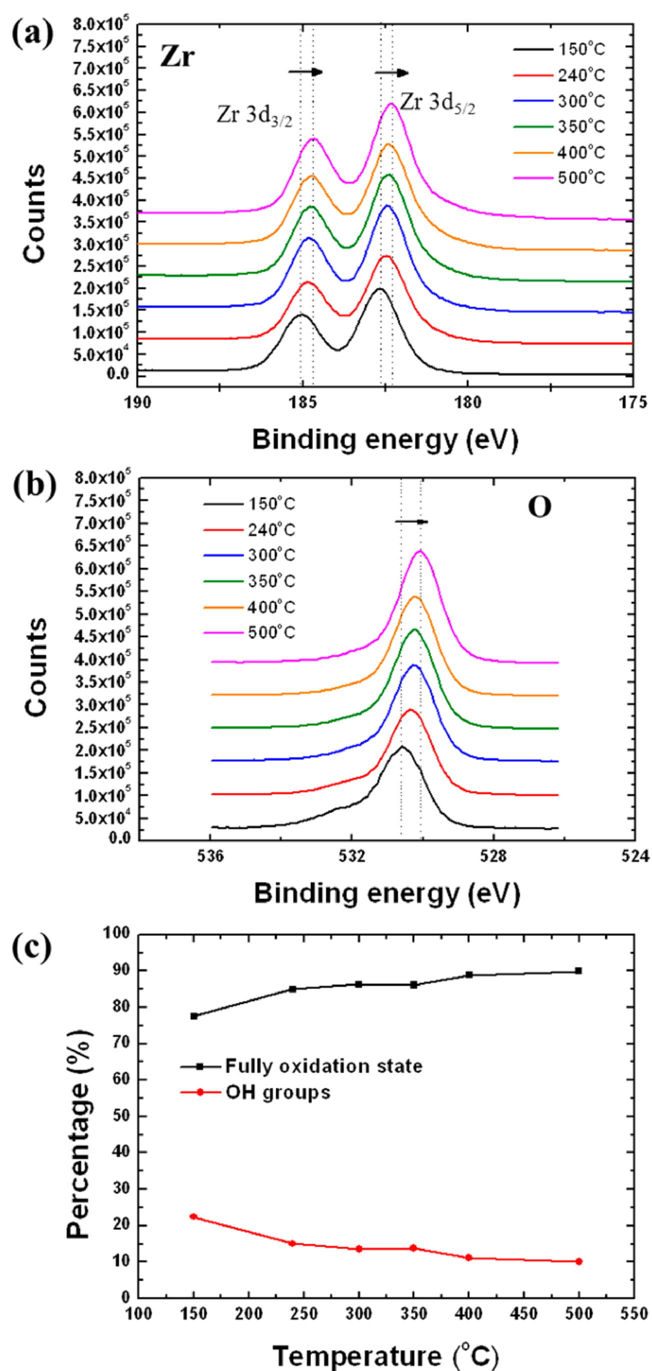

Figure 3. (a) Zr and (b) O peak of the ZrO_2 film as a function of the annealing temperature. (c) Summarized ratios of fully oxidized states and OH groups.

The Zr $3d_{5/2}$ peak is located at 182.2 eV with a fully oxidized state of Zr^{4+} and spin−orbit splitting of 2.1 eV from the Zr $3d_{3/2}$ component (Figure 3a).[30] The 150 °C annealed film was 185.1 eV for the Zr $3d_{5/2}$ and 182.7 eV for the Zr $3d_{3/2}$. As the annealing temperature increased, both peaks shifted to lower binding energies of 184.7 and 182.2 eV, corresponding to Zr $3d_{3/2}$ and Zr $3d_{5/2}$, respectively. This result means that the gradual weight loss of the ZrO_2 solution described in figure 1b was the result of progressive oxidization from $ZrOCl_2$ to ZrO_2. The oxidation behavior is also confirmed by the O 1s peaks (Figure 3b). The O 1s peaks in the ZrO_2 film are shown in Figure 3b, and they can be deconvoluted into two peaks

Table 1. Electrical Characteristics of the MIM Capacitors with a ZrO_2 Dielectric Film Annealed in Air for 2 h

	150 °C	240 °C	300 °C	350 °C	400 °C	500 °C
K (dielectric constant)	8.7	11.1	14.2	14.8	15.0	22.6
J_{leak} (at 2MV/cm)	3.3×10^{-7}	3.5×10^{-5}	7.3×10^{-8}	7.7×10^{-9}	1.4×10^{-8}	9.2×10^{-5}
breakdown voltage (MV/cm)	CL[a]	2.65	2.91	2.8	3.3	3.4

[a]Current limit.

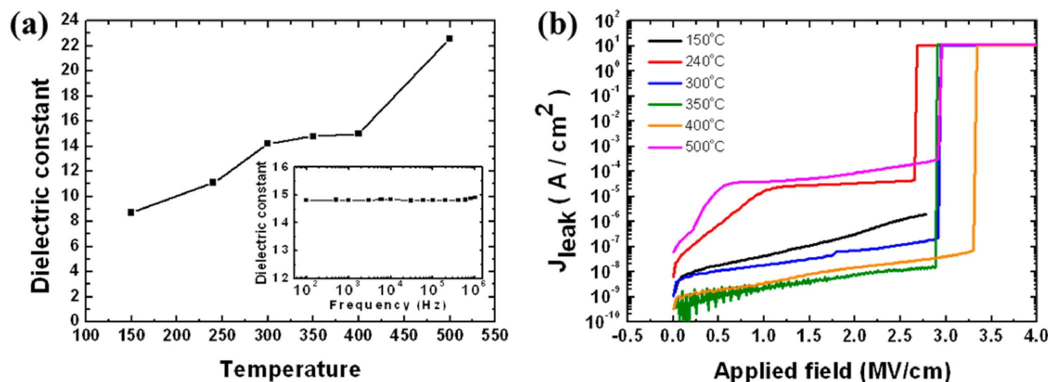

Figure 4. (a) Dielectric constant of the ZrO_2 film vs annealing temperature plots measured at 10 kHz. Inset shows various frequencies vs the dielectric constant of the 350 °C annealed ZrO_2 film. (b) Electric field vs leakage current density of the ZrO_2 film.

corresponding to the OH groups at 531.7 eV and the fully oxidized states at 530.3 eV.[30] As the annealing temperature increased, the O 1s peaks shifted toward the lower binding energy. It is reasonable to assume that hydrolyzed Zr(OH)Cl is converted into ZrO_2 with increasing annealing temperatures. The deconvoluted O 1s peaks, which indicate the OH groups and fully oxidized states, are arranged in Figure 3c. It indicates that the oxidation behavior of the ZrO_2 film and OH groups decreased with increasing annealing temperature.

The dielectric properties were evaluated by fabricating a MIM capacitor structure and are summarized in Table 1. Figure 4a shows the dielectric constant of the ZrO_2 film extracted from capacitance−voltage graphs in Figure S2 in the Supporting Information at a frequency of 10 kHz as a function of the annealing temperature. As the annealing temperature increased, the dielectric constant gradually increased from 8.7 to 22.5. The relatively low dielectric constants of the 150 and 240 °C annealed ZrO_2 films originated from carbon in undecomposed residual solvent or from an imperfect M-O-M frame. Films annealed at temperatures above 300 °C showed reasonable dielectric constants. Especially, the crystallized 500 °C annealed film had a dielectric constant of 22.5. The inset of Figure 4a shows the dielectric constant at various frequencies for the 350 °C annealed film. The mean value of the dielectric constant of the 350 °C annealed film for all frequencies was 14.81 and its standard deviation was just 0.029. This small standard deviation for all the frequencies provides evidence that there were no mobile ions in the film.

Leakage current density (J_{leak}) − electric field (E) measurements were performed to evaluate the leakage current behavior of the ZrO_2 film. The J_{leak} and breakdown voltage of the ZrO_2 film are summarized in Table 1. Interestingly, the 150 °C annealed ZrO_2 film had a relatively low J_{leak} of 3.3×10^{-7} A/cm^2 at 2 MV/cm and it did not show breakdown behavior. This low J_{leak} may come from the relative thick thickness of the film (∼368.5 nm). The 240 °C annealed ZrO_2 film had a high J_{leak} of 3.5×10^{-5} A/cm^2 at 2 MV/cm. The hydroxyl group and residual carbon included in the ZrO_2 film and the lower density film provide a leakage current path, it resulting in a high J_{leak}. The J_{leak} of the ZrO_2 film gradually decreased as the annealing temperature increased from 300 to 400 °C, and the 350 °C annealed ZrO_2 film in particular had the lowest J_{leak} of 7.7×10^{-9} A/cm^2 at 2MV/cm. An abrupt increase in J_{leak} was observed for the 500 °C annealed ZrO_2 film, 9.2×10^{-5} A/cm^2 at 2 MV/cm, which was due to the crystallization of the ZrO_2 film. The presence of grain boundaries resulted in the leakage current path. This crystallization behavior was confirmed by the XRD spectra in Figure 2a. From the results of FT-IR, shown in Figure 2d, the 350 °C annealed ZrO_2 film contains the largest peroxo groups in the film. As the annealing temperature increased, the peroxo groups were partially decomposed and formed Zr−O bonds. We think that peroxo groups in ZrO_2 film decrease defect sites and block leakage current effectively. There are several reported conduction mechanisms through a metal oxide insulator: Schottky emission, Poole−Frenkel emission, Fowler−Nordheim tunneling, and direct tunneling.[31−34] We excluded the conduction mechanism of Schottky emission, Fowler−Nordheim tunneling, and direct tunneling because the thickness of the 350 and 400 °C annealed ZrO_2 films was relatively thick, about 200 nm. All the above-mentioned conduction mechanisms are related to film thickness except Poole−Frenkel emission. Poole-Frenkel emission is a field-assisted thermal detrapping of a carrier that is trapped in a localized state from the bulk oxide into the conduction band. We carefully suggest that peroxo groups decrease the localized state in ZrO_2 films, as evidenced by the fact that the 350 °C annealed ZrO_2 shows lower leakage current density than does the 400 °C annealed ZrO_2 film.

The low J_{leak} in films annealed from 300 to 400 °C is due to the film being dense and its smooth surface. Surface morphology is also important in dielectric films. Smooth surface films have a low J_{leak} because more electric fields are induced in rough surfaces than in smooth surface.[35,36] Furthermore, charge transport in TFTs is confined to the region at the semiconductor/dielectric interface. A rough interface increases interfacial scattering and degrades device

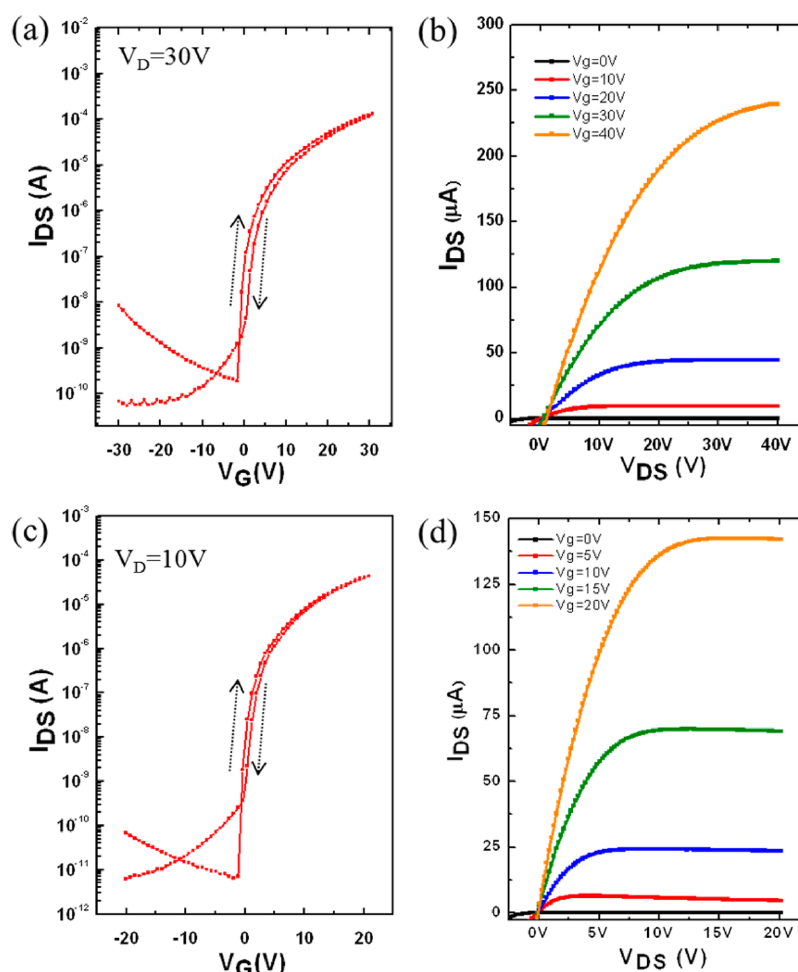

Figure 5. (a) Transfer and (b) output characteristics of the IZO/SiO_2 TFT. (c) Transfer and (d) output characteristics of the IZO/ZrO_2 TFT.

performance. The root-mean-square (rms) of the surface roughness for the 150, 240, 300, 350, 400, and 500 °C annealed ZrO_2 films were 0.153, 0.142, 0.171, 0.126, 0.118, and 0.654 nm, respectively (see Figure S2 in the Supporting Information). All of the films had a very smooth surface with an average value of approximately 0.142 nm until annealing at 500 °C. The slight increase in the rms of the surface roughness of the 500 °C annealed ZrO_2 film is due to the crystallization. This smooth surface may be due to the slow evaporation of the solvent or from products like HCl or Cl_2 gas. Most of the solvent was evaporated in the soft bake process and densification behavior occurred, which was confirmed by the FT-IR results shown in Figure 2d. Residual carbon peaks at 1061 cm^{-1} and a hydroxyl group peak in the range 3000−3500 cm^{-1} present until an annealing temperature of 240 °C. This implies that most of the solvent evaporation and a partial condensation reaction occurred during the soft bake process. The densification process was conducted during the hard bake process, and this densification was confirmed by spectroscopic ellipsometry. As the annealing temperature increased, film density increased until reaching an annealing temperature of 400 °C. Therefore, the surface roughness decreased gradually as the annealing temperature increased to 400 °C, which may result in the low J_{leak} of the ZrO_2 film.

To verify the 350 °C annealed ZrO_2 film as a gate dielectric, bottom-gate-top-contact structures with amorphous IZO TFTs were fabricated on the ZrO_2 film. For comparison, we also fabricated IZO TFTs on thermally grown 200 nm SiO_2. Figure 5 shows the voltage-current curves of the IZO/SiO_2 and IZO/ZrO_2 TFTs. The performances of both devices are summarized in Table 2. Figures 5a and b show a typical transfer and output curve, respectively, of the IZO/SiO_2 TFT, which had a saturation mobility of 2.69 $cm^2/(V\ s)$, a threshold voltage of 4.39 V, a subthreshold slope of 0.501 V/dec, an on/off current ratio of 1.5 × 10^6, and a hysteresis of 1.48 V at a drain voltage (V_D) of 30 V. The transfer and output curve of the IZO/ZrO_2 TFT are shown in figures 5c and d, respectively. The IZO/ZrO_2 TFT had a saturation mobility of 7.21 $cm^2/(V\ s)$, a threshold voltage of 3.22 V, a subthreshold slope of 0.257 V/dec, an on/off current ratio of 6.5 × 10^6, and a hysteresis of 0.58 V at a V_D of 10 V. Both TFTs showed the hysteresis characteristic and their direction was clockwise. There are two hysteresis directions: clockwise and counter clockwise. Clock-

Table 2. Electrical Properties of the IZO/SiO_2 and IZO/ZrO_2 TFTs Annealed at 350°C

TFT	mobility (cm^2/(V s))	threshold voltage (V)	on/off current ratio	subthreshold slope (V/dec)	hysteresis (V)
IZO/SiO_2	2.69	4.39	1.5 × 10^6	0.501	1.48
IZO/ZrO_2	7.21	3.22	6.5 × 10^6	0.257	0.58

wise hysteresis indicates that accumulated electrons are trapped in dielectric/channel interface defect states. Counter clockwise hysteresis reveals that mobile impurity ions exist near the channel region. In the first case, some of the accumulated electrons are transferred into the unoccupied surface states during the forward sweeping of the gate voltage; when gate voltage is backward-sweeping, these states remain filled until the trapped electrons are thermally detrapped. This results in a clockwise hysteresis. In the second case, negative or positive mobile ions result in counterclockwise hysteresis because the slow gate bias response of their motion induces a delay for carrier accumulation or depletion.[37−40] In our system, the IZO/ZrO_2 TFT had clockwise hysteresis, meaning that there were no mobile ions in the ZrO_2 film and that it was fully oxidized. Interestingly, the IZO TFT on the ZrO_2 had higher saturation mobility than the IZO TFT on SiO_2. This increase may have been due to the smooth surface, the high capacitance of the ZrO_2 film, or the enhanced dielectric/channel interface.[41−43]

Finally, to evaluate the electrical stability of the integrated IZO/ZrO_2 TFT, we performed positive gate bias stress (PGBS)-induced stability with a gate voltage of 20 V for 1000 s and recovery behavior was observed; the results are shown in Figure 6. A constant positive gate bias resulted in a

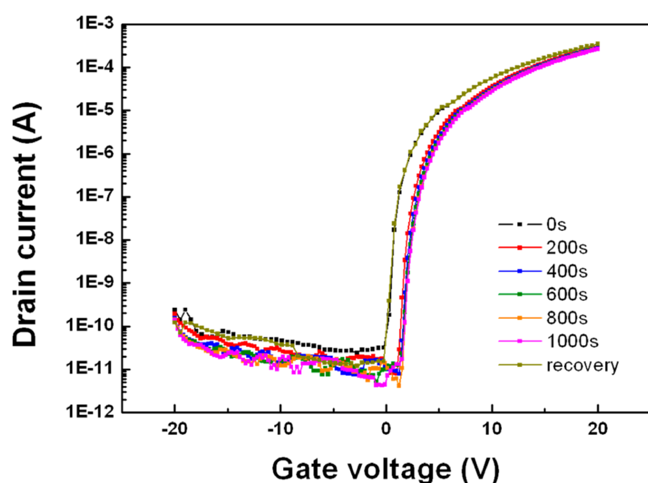

Figure 6. Evaluation with positive gate bias stress of the IZO/ZrO_2 TFT at a gate voltage of 20 V for 1000 s and its recovery behavior.

positive shift of 1.6 V for the threshold voltage and a return to its original position after 10 min, turning off the bias stress. This positive shift of the threshold voltage can be explained by charge trapping at the dielectric/channel interface or by charge injected into the dielectric.[44] This small shift in the threshold voltage indicates that there are a small number of defect states at the dielectric/channel interface. Moreover, the subthreshold slope of the device did not change even after the device had undergone bias stressing. This indicates that no additional defect states were created at the channel/dielectric interface after the device was stressed. To verify the low interface state of IZO TFT on ZrO_2 dielectric, we fabricated metal-oxide-semiconductor (MOS) capacitor with structure of Al/IZO/ZrO_2/P^{2+} Si and measured capacitance−voltage curves as a function of frequencies. It shows negligible hysteresis of $C-V$ curves, indicating low interface trap density between channel and dielectric (see Figure S4 in the Supporting Information).

Although we successfully demonstrated a solution-processed IZO TFT on a ZrO_2 dielectric with a thickness of 210 nm, the operating voltage and thickness of the ZrO_2 is relatively high. To reduce ZrO_2 thickness, we controlled the solution concentration to between 0.05 and 0.2 M under fixed spin-coating conditions of 3000 rpm for 20 s. To evaluate the electrical properties of the thin ZrO_2, we fabricated an Al/ZrO_2/P^{2+} Si structure. The film thickness and its corresponding leakage current density at 1 MV/cm are shown in Figure S5a in the Supporting Information with various numbers of layers. The film thickness increased linearly with the number of layers. All films showed a low leakage current density of approximately 1×10^{-8} A/cm^2 at 1 MV/cm. Figure S5b in the Supporting Information shows the capacitances of the thin ZrO_2 dielectric at 1 kHz with various numbers of layers, and 0.2 M ZrO_2 solution with a three coat layer was chosen for low operating voltage IZO TFTs. Finally, we operated IZO TFTs on a 52 nm thick ZrO_2 film and they were capable of operating even at a 3 V operating voltage (see Figure S5c, d in the Supporting Information). The IZO TFTs had a mobility of 2.72 cm^2/(V s), a threshold voltage of 0.22 V, an on/off current ratio of 7.12×10^5, a subthreshold slope of 0.188 V/dec, and a hysteresis of 0.09 V at a V_D of 3 V. This implies that a thin peroxo-ZrO_2 dielectric can operate IZO TFTs at low operating voltages and that it has a high switching speed.

4. CONCLUSION

Herein, we demonstrated the fabrication of a solution-processed metal oxide TFTs based on a peroxo-ZrO_2 dielectric film at an annealing temperature of 350 °C, and we verified the formation of peroxo-ZrO_2 films at various annealing temperatures through TG-DTA, FT-IR, and XPS analysis tools. Hydrogen peroxide makes the peroxo species in the ZrO_2 film and forms the dense film. This peroxo species was verified by FT-IR. Finally, we integrated an IZO/ZrO_2 TFT and compared its properties to an IZO/SiO_2 TFT. The IZO/ZrO_2 TFT had a saturation mobility of 7.21 cm^2/(V s) and only a 1.6 V shift occurred under PGBS conditions. Therefore, effective low-temperature solution-processed TFTs can be realized with hydrogen peroxide, and the process described the makes the fabrication of devices on commercial glass easier.

■ ASSOCIATED CONTENT

Supporting Information

Cross-sectional SEM images, AFM images of ZrO_2 films, and capacitance−voltage curves of ZrO_2 film annealed at various temperatures. The ZrO_2 film thickness and its corresponding leakage current density at 1 MV/cm with various solution concentrations as a function of numbers of layers. The capacitances of the thin ZrO_2 dielectric at 1 kHz with various numbers of layers. Transfer and output curves of IZO TFT with 52 nm ZrO_2 dielectric. This material is available free of charge via the Internet at http://pubs.acs.org.

■ AUTHOR INFORMATION

Corresponding Author

*Phone: +82-10-9043-2838. E-mail: thinfilm@yonsei.ac.kr.

Notes

The authors declare no competing financial interest.

■ ACKNOWLEDGMENTS

This work was supported by the National Research Foundation of Korea (NRF, 2012-0008721) funded by the government of Korea (MEST). Further funding came from LG Display.

REFERENCES

(1) Banger, K. K.; Yamashita, Y.; Mori, K.; Peterson, R. L.; Leedham, T.; Rickard, J.; Sirringhaus, H. *Nat. Mater.* **2011**, *10*, 45−50.
(2) Kim, M. G.; Kanatzidis, M. G.; Facchetti, A.; Marks, T. J. *Nat. Mater.* **2011**, *10*, 382−388.
(3) Park, J. H.; Choi, W. J.; Oh, J. Y.; Chae, S. S.; Jang, W. S.; Lee, S. J.; Song, K. M.; Baik, H. K. *Jpn. J. Appl. Phys.* **2011**, *50*, 070201.
(4) Meyers, S. T.; Anderson, J. T.; Hung, C. M.; Thompson, J.; Wager, J. F.; Keszler, D. A. *J. Am. Chem. Soc.* **2008**, *130*, 17603−9.
(5) Kim, G. H.; Shin, H. S.; Ahn, B. D.; Kim, K. H.; Park, W. J.; Kim, H. J. *J. Electrochem. Soc.* **2009**, *156*, H7−H9.
(6) Kim, K. M.; Kim, C. W.; Heo, J. S.; Na, H.; Lee, J. E.; Park, C. B.; Bae, J. U.; Kim, C. D.; Jun, M.; Hwang, Y. K.; Meyers, S. T.; Grenville, A.; Keszler, D. A. *Appl. Phys. Lett.* **2011**, *99*, 242109.
(7) Rim, Y. S.; Jeong, W. H.; Kim, D. L.; Lim, H. S.; Kim, K. M.; Kim, H. J. *J. Mater. Chem.* **2012**, *22*, 12491−12497.
(8) Lee, M. S.; An, C. H.; Lim, J. H.; Joo, J. H.; Lee, H. J.; Kim, H. J. *J. Electrochem. Soc.* **2010**, *157*, G142−G146.
(9) Pal, B. N.; Dhar, B. M.; See, K. C.; Katz, H. E. *Nat. Mater.* **2011**, *10*, 45−50.
(10) Adamopoulos, G.; Thomas, S.; Bradley, D. D. C.; McLachlan, M. A.; Anthopoulos, T. D. *Appl. Phys. Lett.* **2011**, *98*, 123503.
(11) Meyers, S. T.; Anderson, J. T.; Hong, D.; Hung, C. M.; Wager, J. F.; Keszler, D. A. *Chem. Mater.* **2007**, *19*, 4023−4029.
(12) Jiang, K.; Anderson, J. T.; Hoshino, K.; Li, D.; Wager, J. F.; Keszler, D. A. *Chem. Mater.* **2011**, *23*, 945−952.
(13) Avis, C.; Jang, J. *J. Mater. Chem.* **2011**, *21*, 10649−10652.
(14) Kim, S. J.; Yoon, D. H.; Rim, Y. S.; Kim, H. J. *Electrochem. Solid-State Lett.* **2011**, *14*, E35−E37.
(15) Zhu, L. Q.; Fang, Q.; He, G.; Liu, M.; Zhang, L. D. *Mater. Lett.* **2006**, *60*, 888−891.
(16) Goedicke, K.; Liebig, J. S.; Zywitzki, U. O.; Sahm, H. *Thin Solid Films* **2000**, *37*, 377−378.
(17) Scholes, F. H.; Hughes, A. E.; Hardin, S. G.; Lynch, P.; Miller, P. R. *Chem. Mater.* **2007**, *19*, 2321−2330.
(18) Picquart, M.; López, T.; Gómez, R.; Torres, E.; Moreno, A.; Garcia, J. *J. Therm. Anal. Calorim.* **2004**, *76*, 755−761.
(19) Zhu, M.; Chen, P.; Fu, R. K.Y.; Liu, W.; Lin, C.; Chu, P. K. *Thin Solid Films* **2005**, *476*, 312−316.
(20) Lu, C. H.; Raitano, J. M.; Khalid, S.; Zhang, L.; Chan, S. W. *J. Appl. Phys.* **2008**, *103*, 124303.
(21) Anderson, J. T.; Munsee, C. L.; Hung, C. M.; Phung, T. M.; David, G. S. H.; Johnson, C.; Wager, J. F.; Keszler, D. A. *Adv. Funct. Mater.* **2007**, *17*, 2117−2124.
(22) Venkataraj, S.; Kappertz, O.; Weis, H.; Drese, R.; Wuttig, M. *J. Appl. Phys.* **2002**, *92*, 3599.
(23) Mergel, D. *Thin Solid Films* **2001**, *397*, 216−222.
(24) Ochando, I. M.; Vila, M.; Prieto, C. *Vacuum* **2007**, *81*, 1484−1488.
(25) Niinistö, J.; Putkonen, M.; Niinisto, L.; Kukli, K.; Ritala, M.; Leskela, M. *J. Appl. Phys.* **2004**, *95*, 84.
(26) Socrates, G. *Infrared Characteristic Group Frequencies: Tables and Charts*, 3rd ed.; John Wiley & Sons: New York, 1994; Vol. *6*, p 94.
(27) Shearer, J.; Scarrow, R. C.; Kovacs, J. A. *J. Am. Chem. Soc.* **2002**, *124*, 11709−11717.
(28) Powers, D. A.; Gray, H. B. *Inorg. Chem.* **1973**, *12*, 2721−2726.
(29) Agarwal, M.; Guire, M. R. D.; Heuer, A. H. *J. Am. Ceram. Soc.* **1997**, *80*, 2967−2981.
(30) Valov, I.; Stoychev, D.; Marinova, T. *Electrochim. Acta* **2002**, *47*, 4419−4431.
(31) Yang, B. L.; Lai, P. T.; Wong, H. *Microelectron. Reliab.* **2007**, *44*, 709−718.
(32) Mead, C. A. *Phys. Rev.* **1962**, *128*, 2088−2093.
(33) Cheong, K. Y.; Moon, J. H.; Kim, H. J.; Bahng, W.; Kim, N. *J. Appl. Phys.* **2008**, *103*, 084113.
(34) Chiu, F.; Wang, J.; Lee, J. Y.; Wu, S. C. *J. Appl. Phys.* **1997**, *81*, 6911.
(35) Zhao, Y. P.; Wang, G. C.; Lu, T. M. *Phys. Rev. B* **1999**, *60*, 9157−9164.
(36) Haspert, L. C.; Lee, S. B.; Rubloff, G. W. *ACS Nano* **2012**, *6*, 3528−3536.
(37) Niahii, J.; Ohtomo, A.; Ohtani, K.; Ohno, H.; Kawasaki, M. *Jpn. J. Appl. Phys.* **2005**, *44*, L1193−L1195.
(38) Snow, E. H.; Grove, A. S.; Deal, B. E.; Sah, C. T. *J. Appl. Phys.* **1965**, *36*, 1664−1673.
(39) Chanthaphan., A.; Hosoi, T.; Mitani, S.; Nakano, Y.; Nakamura, T.; Shimura, T.; Watanabe, H. *Appl. Phys. Lett.* **2012**, *100*, 252103.
(40) Liu, J.; Buchholz, D. B.; Hennek, J. W.; Chang, R. P. H.; Facchetti, A.; Marks, T. J. *J. Am. Chem. Soc.* **2010**, *132*, 11934−11942.
(41) Nayak, P. K.; Hedhili, M. N.; Cha, D.; Alshareef, H. N. *Appl. Phys. Lett.* **2012**, *100*, 202106.
(42) Wang, L.; Yoon, M. H.; Lu, G.; Yang, Y.; Facchetti, A.; Marks, T. J. *Nat. Mater.* **2006**, *5*, 893−900.
(43) Adamopoulos, G.; Thomas, S.; Wöbkenberg, P. H.; Bradley, D. D. C.; McLachlan, M. A.; Anthopoulos, T. D. *Adv. Mater.* **2011**, *23*, 1894−1898.
(44) Schaeffer, J. K.; Gilmer, D. C.; Samavedam, S.; Raymond, M.; Haggag, A.; Kalpat, S.; Steimle, B.; Capasso, C.; White, B. E. *J. Appl. Phys.* **2007**, *102*, 074511.